

Electrical, microstructural, and thermal stability characteristics of Ta/Ti/Ni/Au contacts to *n*-GaN

Abhishek Motayed

Department of Electrical Engineering, Howard University, Washington, DC 20059

Kenneth A. Jones, Michael A. Derenge, and Mark C. Wood

U.S. Army Research Laboratory, Mail Stop AMSRL-SE-RL, Adelphi, Maryland 20783

D. N. Zakharov and Z. Liliental-Weber

Lawrence Berkeley National Laboratory, M.S. 62-203, Berkeley, California 94720

David J. Smith

Department of Physics and Astronomy, Arizona State University, Tempe, Arizona 85287

Albert V. Davydov

U.S. National Institute of Standards and Technology, Metallurgy Division, 8555, Gaithersburg, Maryland 20899

Wallace T. Anderson

Electronic Sciences and Technology Division, U.S. Naval Research Laboratory, Washington, DC 20375

Agis A. Iliadis

Department of Electrical and Computer Engineering, University of Maryland, College Park, Maryland 20742

S. Noor Mohammad^{a)}

Department of Electrical Engineering, Howard University, Washington, DC 20059

(Received 16 June 2003; accepted 20 October 2003)

A metallization technique has been developed for obtaining low resistance Ohmic contact to *n*-GaN. The metallization technique involves the deposition of a metal layer combination Ta/Ti/Ni/Au on an *n*-GaN epilayer. It is observed that annealing at 750 °C for 45 s leads to low contact resistivity. Corresponding to a doping level of $5 \times 10^{17} \text{ cm}^{-3}$, the contact resistivity of the contact $\rho_s = 5.0 \times 10^{-6} \Omega \text{ cm}^2$. The physical mechanisms underlying the realization of low contact resistivity is investigated using current–voltage characteristics, x-ray diffraction, Auger electron spectroscopy, transmission electron microscopy, and energy dispersive x-ray spectrometry.

© 2004 American Institute of Physics. [DOI: 10.1063/1.1633660]

I. INTRODUCTION

The last several years have witnessed a very rapid progress in the III–V nitride materials and technology for both microelectronic and optoelectronic applications. The success of III–V nitride devices rests largely on the realization of high-performance metal/semiconductor (M/S) contacts. Many different metals and metal combinations have been tried to obtain these contacts.^{1–12} Tantalum (Ta), which was also used for this purpose, is known to react¹³ with AlGaIn to form nitrides. Ta-based metallization referred to as an “advancing interface contact scheme” has been used to form source and drain contacts to AlGaIn/GaN high electron mobility transistors. It has been observed that, upon rapid thermal annealing (RTA), a part of the AlGaIn barrier layer is consumed by the reaction between Ta and the AlGaIn alloy. Such a reaction modifies the interface between the metal and the semiconductor. The carrier tunneling from the source/drain regions to the channel region is thus enhanced.

In this article we describe the electrical, microstructural, and thermal stability properties of a multilayer Ta/Ti/Ni/Au contact (see Fig. 1) metallization scheme developed to form low resistance Ohmic contacts to *n*-GaN. One primary objective is to investigate the combined nitride forming effect of Ta and Ti in the reaction with *n*-GaN. It is expected that the carrier tunneling facilitated by this reaction will lead to the creation of a low resistance Ohmic contact. Both Ta and Ti metals are known to react with GaN and AlGaIn, forming TaN and TiN, respectively.^{14,15} Although the Ta/Ti metallization scheme has been used successfully to form Ohmic contacts^{16,17} to *p*-GaN, no Ta/Ti metallization seems to have been made for the Ohmic contact to *n*-GaN. The basic idea underlying the Ta/Ti/Ni/Au multilayer contact is that the thin Ta layer in intimate contact with *n*-GaN, and a Ti layer on the top of the Ta layer, would undergo a substantial solid phase reaction with *n*-GaN during RTA of the structure, producing low resistance Ohmic contacts. As may be noted¹⁸ from Table I, tantalum has a work function of 4.25 eV, which is sufficient to produce Schottky contacts to *n*-GaN. In general, Schottky contacts have nonlinear current–voltage (*I*–*V*) characteristics.

^{a)}Summer Faculty Fellow, U.S. Naval Research Laboratory, Washington, DC 20375; author to whom correspondence should be made; electronic mail: snmohammad2002@yahoo.com

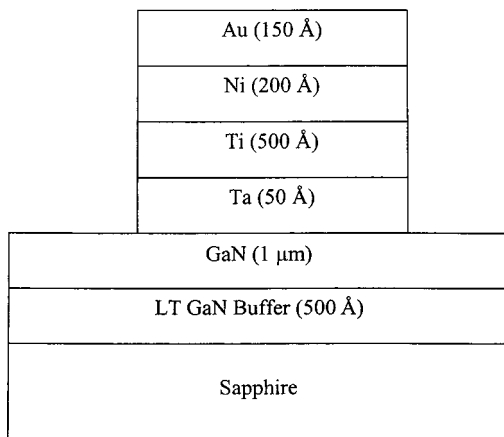


FIG. 1. Schematic layer structure of an *n*-GaN/Ta/Ti/Ni/Au contact structure.

II. EXPERIMENTAL METHOD

The GaN films for this study were grown at the U.S. Army Research Laboratory, Adelphi, MD, by the metal organic chemical vapor deposition method on (0001) sapphire substrates, about 400 μm thick. First, an undoped low temperature, 30-nm-thick, GaN buffer layer was deposited on the substrate. Then, a Si-doped GaN epilayer, about 1 μm thick, was grown on a GaN buffer layer by using an 8 sccm flow of silane. Prior to the processing of the samples, these were cleaned using the standard procedure that involves a 3 min heated ultrasonic bath, successively, in trichloroethylene, acetone, and methanol. The samples were then dipped in a heated bath of $\text{NH}_4\text{OH}:\text{H}_2\text{O}_2:\text{H}_2\text{O}$ (1:1:5) for 3 min. It was followed by a 3 min dip in a heated $\text{HCl}:\text{H}_2\text{O}_2:\text{H}_2\text{O}$ (1:1:5) mixture. Mesa structures for transmission line measurement (TLM) for the Ohmic contacts were created by reactive ion etching (RIE) of the GaN epilayer. A Plasma-Therm 790 Series chamber was employed for this purpose. The RIE was accomplished by flowing Cl_2 gas at 15 sccm for 4 min. The operating pressure was 10 mTorr, and the power was 150 W. Samples were patterned for TLM pads. After photolithography, the samples were dipped into a $\text{HF}:\text{HCl}:\text{H}_2\text{O}$ (1:1:10) mixture for 15 s, rinsed in deionized water, and blown dried. They were loaded immediately for metal deposition. The composite metal layer deposited on *n*-GaN was Ta/Ti/Ni/Au (50 Å/500 Å/200 Å/150 Å). All the

TABLE I. Work functions, melting points, and resistivities of various metals.

Metal	Work function (eV)	Melting point (°C)	Resistivity ($\Omega\text{ cm}$)
Ga	3.96
Al	4.25	660	2.65×10^{-6}
Ti	3.95	1668	4.20×10^{-6}
Ni	4.50	1453	6.84×10^{-6}
Au	4.30	1063	2.35×10^{-6}
Ta	4.25
Pd	5.12	1552	1.08×10^{-5}
TiN	3.74	...	1.00×10^{-5}
TaN, ZrN, VN, NbN	>4.00	...	2.25×10^{-4}

metals, except Au, were deposited by electron beam evaporation. Au was evaporated thermally. Following the metallization, metal lift-off was performed in acetone, which provided a linear configuration of pads with (300 $\mu\text{m} \times 300 \mu\text{m}$) dimension. The pad spacings were 2, 5, 10, 15, 20, 30, 40, 50, 60, and 90 μm , respectively. RTA of the samples was then performed in argon gas at various temperatures. Argon removed the oxygen and water vapor from the furnace, reducing the oxidation probability of the contacts. *I*-*V* characteristics of the contact layers were measured before and after RTA. The TLM measurement of the Ohmic contact was performed for those contacts that had linear *I*-*V* characteristics.

III. ELECTRICAL CHARACTERISTICS

A. Electrical characteristics

Figure 1 shows that the present contact metallization scheme utilizes a relatively thin layer (50–80 Å) of Ta in contact with *n*-GaN. Electrical characteristics of the contacts were studied as functions of RTA temperature and RTA time. The effect of the tantalum layer thickness on the electrical characteristics was also studied. Three different Ta layer thicknesses were used for this purpose. As-deposited contacts exhibited nonlinear *I*-*V* characteristics, as shown in Fig. 2(a). This was expected considering that Ta has a work function of 4.25 eV as compared to the GaN electron affinity of 4.10 eV. It is, however, evident from Figs. 2(b)–2(d) that the present metallization turned Ohmic after annealing at 750 °C. Contacts after annealing at 550 °C showed marginal or no improvement in the *I*-*V* characteristics. This is because there was essentially no reaction between GaN and the metals yielding reaction products with work functions comparable to that of GaN. That these products were indeed formed after a RTA at 750 °C for 45 s was evident from the linear *I*-*V* characteristics and a fairly low value of contact resistance.

B. Contact resistance

Contact resistances were determined based on the TLM method. Mesas were defined to eliminate current flow at the contact edge. The resistance, R_T , between two contacts was measured at 300 K using a four-point-probe arrangement. The specific contact resistance (hereafter, referred to as contact resistivity) ρ_S was derived from the R_T versus gap length plots. The method of least squares was used to fit a straight line to the experimental data, which were obtained from all available test patterns.

Table II summarizes the effect of annealing on the contact resistivity of various contacts. From Table II, it is evident that the contact resistivity depends on the RTA temperature of the sample. The lowest contact resistivity of the Ta/Ti/Ni/Au (50 Å/500 Å/200 Å/150 Å) contacts was in the range of $5.0 \times 10^{-6} \Omega\text{ cm}^2$ after RTA at 750 °C for 45 s. Increasing the RTA time accompanied an increased contact resistivity. Increasing the RTA temperature beyond 775 °C had, however, a marginal effect on the contact resistivity. While the contact with 80-Å-thick Ta had contact resistivity essentially the same as that of the contact with 50 Å Ta under

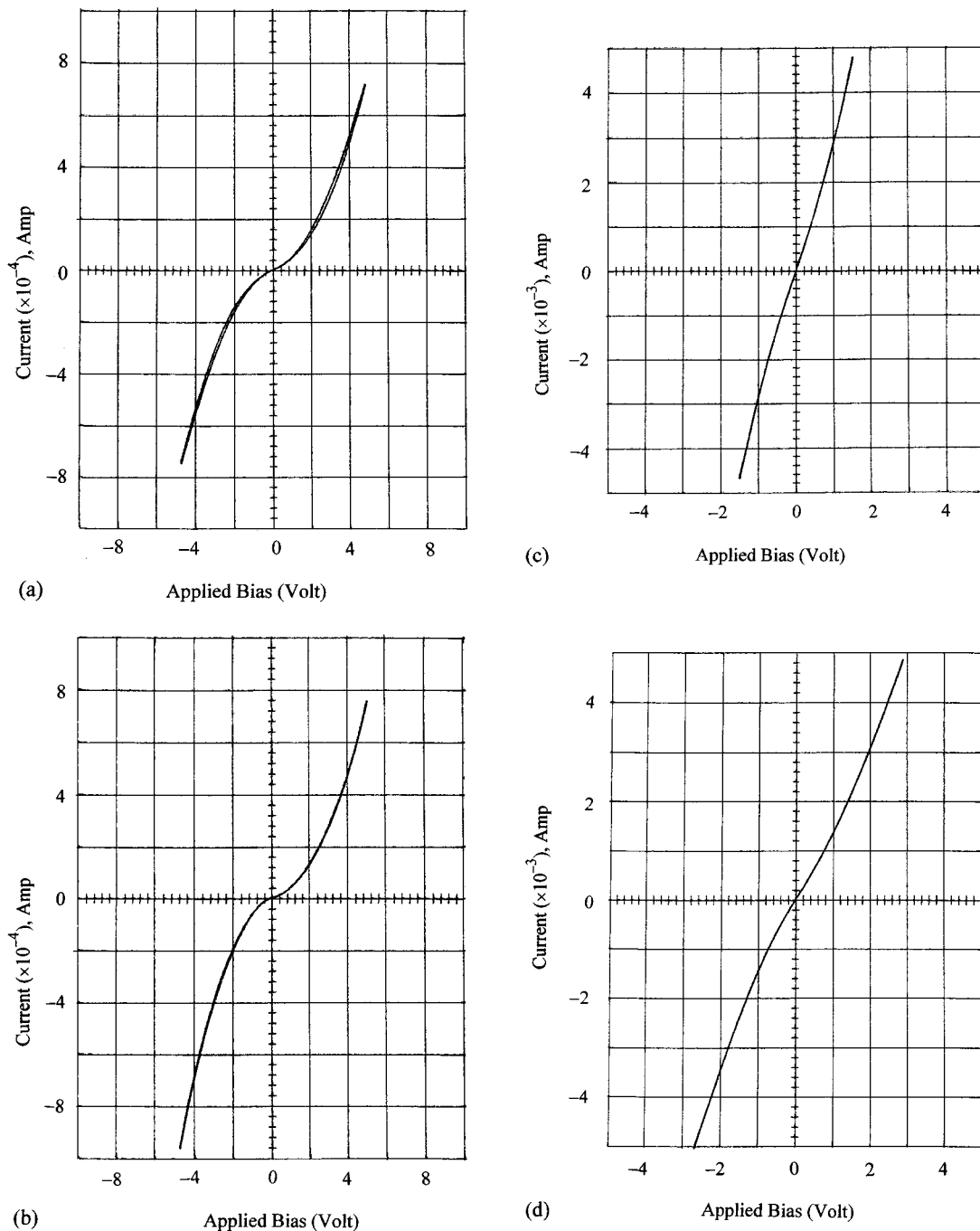


FIG. 2. Current–voltage characteristics of Ta/Ti/Ni/Au (50 Å/500 Å/200 Å/150 Å) contacts (a) as deposited (b) annealed at 550 °C for 45 s, (c) annealed at 750 °C for 45 s, and (d) annealed at 775 °C for 45 s.

identical annealing conditions, contacts with 25-Å-thick Ta failed to show Ohmic behavior even after RTA at 750 °C. The optimum metal thickness for the Ta/Ti/Ni/Au metallization was (50 Å/500 Å/200 Å/150 Å) with an optimum RTA condition of 750–775 °C for 45 s.

IV. MICROSTRUCTURE

In order to carry out microstructural analysis of the contact layers, we performed x-ray diffraction (XRD), Auger electron spectroscopy (AES), transmission electron microscopy (TEM), and energy dispersive x-ray spectrometry

(EDX), which are described below. Various structures used for this study are shown in Table II as samples 1–9.

A. X-ray diffraction analysis

XRD analysis was carried out for the Ta/Ti/Ni/Au microstructure annealed at two different temperatures. The objective was to better understand the reaction mechanism involved in the Ohmic contact formation. Investigation of the phase formation at these two temperatures showed significant changes of contact resistances. Figure 3 displays the XRD spectra of the GaN/Ta/Ti/Ni/Au (50 Å/500 Å/200 Å/150 Å) contact annealed at 750 and 775 °C, respectively,

TABLE II. Specific contact resistance of various Ta/Ti/Ni/Au microstructures annealed at various temperatures and for various time periods.

Sample	Ta/Ti/Ni/Au contact thickness	Annealing temperature (°C)	Annealing time (s)	I-V characteristics	Contact resistivity ($\Omega \text{ cm}^2$)
1	Ta/Ti/Ni/Au 50 Å/500 Å/200 Å/150 Å	As deposited	...	Nonlinear	...
2	Ta/Ti/Ni/Au 50 Å/500 Å/200 Å/150 Å	550	45	Nonlinear	...
3	Ta/Ti/Ni/Au 50 Å/500 Å/200 Å/150 Å	750	45	Linear	5.0×10^{-6}
4	Ta/Ti/Ni/Au 50 Å/500 Å/200 Å/150 Å	750	60	Linear	1.2×10^{-5}
5	Ta/Ti/Ni/Au 50 Å/500 Å/200 Å/150 Å	775	45	Linear	6.0×10^{-5}
6	Ta/Ti/Ni/Au 80 Å/500 Å/200 Å/150 Å	As deposited	...	Nonlinear	...
7	Ta/Ti/Ni/Au 80 Å/500 Å/200 Å/150 Å	750	45	Linear	5.6×10^{-6}
8	Ta/Ti/Ni/Au 25 Å/500 Å/200 Å/150 Å	As deposited	...	Nonlinear	...
9	Ta/Ti/Ni/Au 25 Å/500 Å/200 Å/150 Å	750	45	Nonlinear	...

for 45 s. The Ta/Ti/Ni/Au (50 Å/500 Å/200 Å/150 Å) contacts annealed at 750 °C had contact resistivity on the order of $5 \times 10^{-6} \Omega \text{ cm}^2$. However, the same contact annealed at 775 °C had a much higher contact resistivity. The XRD pattern for the samples annealed at 750 °C indicated that the observed Au(111) peak was at the $38.34^\circ 2\theta$ position, which corresponded to a lattice parameter $a = 4.066 \text{ \AA}$. For pure Au(111), this peak was at 38.22° with $a = 4.078 \text{ \AA}$. The peak shift from 38.34° to 38.22° resulted from Au forming solid solution with other metals. Although the solute metal (SM) atom radius r_{SM} may be different from the host lattice (HL)

atom radius r_{HL} , the solute metal atoms do substitute host lattice sites in a solid solution. Such a substitution causes a reduction in the host lattice parameter if $r_{SM} < r_{HL}$. On this ground, Ni and Ti ($a_{Ni} = 3.5238 \text{ \AA}$, $a = 2.95 \text{ \AA}$) dissolved in Au led to a decrease in the lattice parameter of pure Au. The appearance of a distinct peak with relatively high intensity at the $42.93^\circ 2\theta$ ($d = 2.104 \text{ \AA}$) position was observed in the sample annealed at 775 °C. This peak was attributed to 200 reflection of the fcc (Ti,Ta) N_{1-y} phase. Note that the 2θ value of this peak corresponded to $a_{fcc} = 4.208 \text{ \AA}$, which is

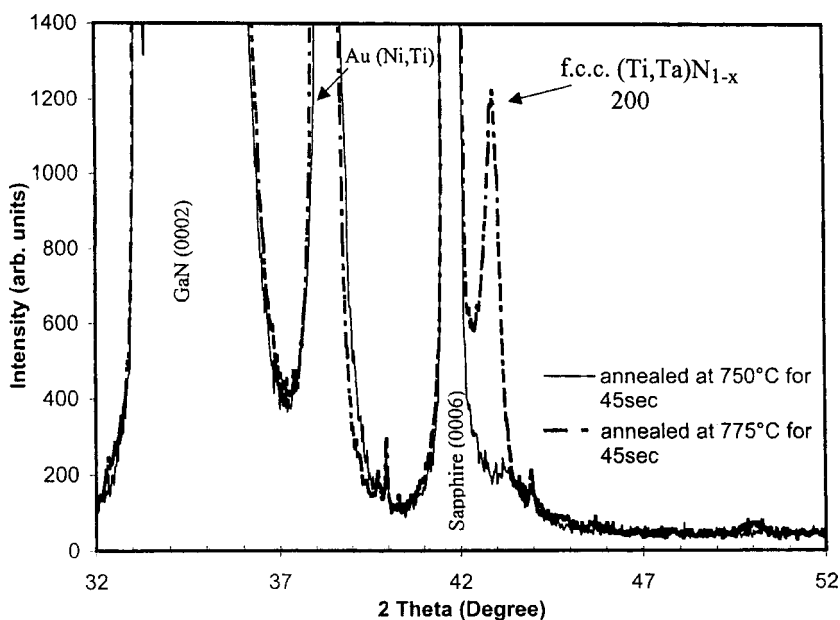


FIG. 3. X-ray diffraction pattern of Ta/Ti/Ni/Au (50 Å/500 Å/200 Å/150 Å) contacts annealed at different temperatures.

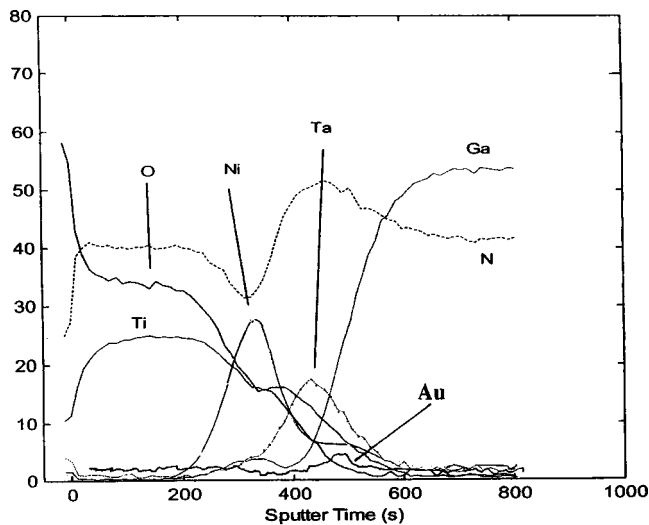


FIG. 4. Auger electron spectroscopy depth profiles of Ta/Ti/Ni/Au (50 Å/500 Å/200 Å/150 Å) contacts annealed at 750 °C for 45 s.

very close to $a_{\text{fcc}} = 4.200 \text{ \AA}$ for the nitrogen deficient TiN_{1-y} phase.¹⁹ The presence of Ta in the Ti sublattice thus brought about a slight lattice expansion of the $(\text{Ti,Ta})\text{N}_{1-y}$ phase. More light could be shed on it with the availability of the data correlating the lattice parameter and composition of the metal nitride phases. Although the presence of nitrides could not be ascertained in the microstructure solely on the basis of XRD analysis, formation of mixed (Ti,Ta) nitrides was found to be thermodynamically favorable. Enthalpies of formation of TiN and TaN are -338 and -251 KJ/g atom , respectively.²⁰ Comparing these values with the enthalpy of formation of GaN (-110 KJ/gm atom), it can be concluded that indeed these reactions might have occurred, as these were thermodynamically favorable. Notably, the (111) peak of Au in the Ta/Ti/Ni/Au multilayer annealed at 775 °C shifted towards the right, indicating a decrease in the lattice parameter. This is quite reasonable because, at higher temperature, Au dissolved more Ni and Ti, leading to a further reduction in its lattice parameter.

B. Auger electron spectroscopic analysis

The AES depth profile of the Ta/Ti/Ni/Au (50 Å/500 Å/200 Å/150 Å) contact annealed at 750 °C for 45 s is shown in Fig. 4. The AES depth profile reveals that an appreciable amount of interdiffusion took place between various metal layers. A notable feature of the microstructure was the intermixing of the metal layers upon RTA. Although intermixing of Ta and Ti could be clearly seen from the AES plot, the Ta signal was not broadened nor spread out throughout the microstructure. This implied that the outdiffusion of Ta was rather minimal. This is important because such structural integrity is crucial for the formation of reliable contacts. A similar effect was also observed with the Ni layer. Another important observation was the diffusivity of Ti towards the multilayer metal surface, and the formation of oxides upon RTA. In an earlier investigation²¹ on the Ti/Au/Pd/Au microstructure, it was observed that Ti was driven outwards under the influence of the reaction kinetics of the oxide forming

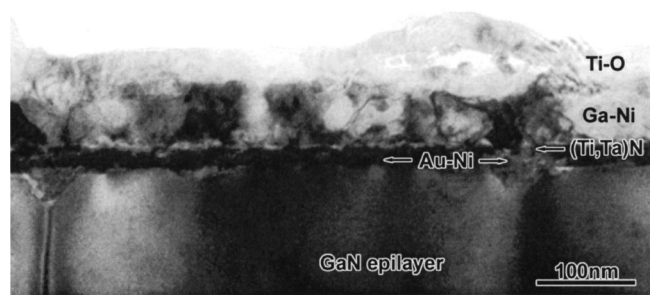


FIG. 5. TEM bright-field image of the sample 3 annealed at 750 °C. White arrows show V-shaped pits formed at the dislocation line facing the GaN surface. The extreme left of the epilayer shows a funnel-shaped nanopipe.

reaction. To overcome this, in the present experiment, the RTA chamber was purged several times, each time for a long period.

C. TEM and EDX analyses

TEM and EDX analyses were carried out to understand the microstructure of the annealed samples. There was also a need, for example, to understand why the Ta/Ti/Ni/Au (5 nm/50 nm/20 nm/15 nm) system deposited on an *n*-GaN epilayer, and annealed at 750 and 775 °C, respectively, shows almost an order of magnitude difference in the contact resistivity: $5 \times 10^{-6} \Omega \text{ cm}^2$ for sample 3, and $6 \times 10^{-5} \Omega \text{ cm}^2$ for sample 5 (see Table II).

The TEM bright-field (BF) image (Fig. 5), together with the EDX line profiles [Figs. 6(a) and 6(b)] of the sample 3 Ohmic contact, reveals again extensive diffusion of various deposited layers. Several new layers, including the Au–Ni layer, followed by Ti–Ta, Ni–Ga, and Ti–O layers, respectively, were formed onto the GaN surface upon RTA. The first layer, consisting of Au–Ni microcrystals, was embedded onto the GaN surface. With GaN decomposing during annealing, the Au–Ni crystals grew in size forming a pseudo-continuous layer, up to 30 nm in thickness. Pores or V-shaped pits²² were also formed at dislocations intersecting the GaN surface (marked by arrows in Fig. 5). The decomposition of GaN during RTA caused Ga atoms to outdiffuse, and to form polycrystalline Ni–Ga with N distributed somewhere in the sample. A comparison of the TEM BF image (Fig. 5) of the contact area of sample 3 and electron energy loss (EEL) spectroscopic images²³ for this suggests that Ti and N were present within the originally deposited Ta layer. This layer was about 5–8 nm thick, as confirmed by high-resolution electron microscopic (HREM) images [Fig. 7(a)]. Further, some of the Ti diffused to the surface leaving only a thin stripe in its original location. The presence of oxygen in both the locations suggested that Ti–O was formed almost everywhere; the $(\text{Ti,Ta})\text{N}$ layer was formed only at the GaN interface. Argon gas used during annealing is attributed to be the source of this oxygen. Ta showed essentially no tendency to outdiffuse into Ti, Ni, and Au.

The HREM image [Fig. 7(a)] shows that the surface of undecomposed GaN is approximately at the same level as the interface between the Au–Ni and the $(\text{Ti,Ta})\text{N}$ [right part of Fig. 7(a)] alloys. This implies that the Au–Ni alloy was em-

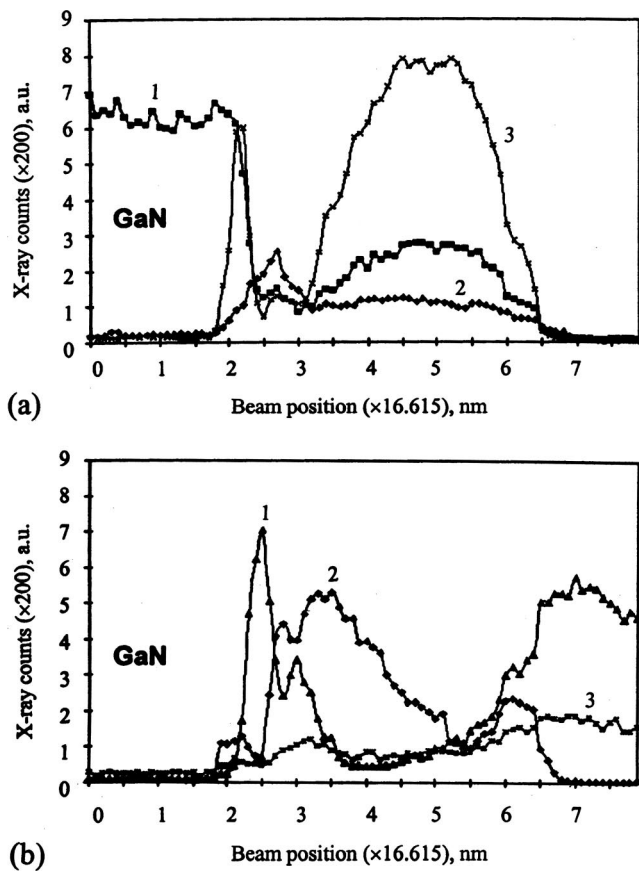


FIG. 6. EDX line profile spectra showing the element distribution across the contact; (a) element distribution of Ta, Ga, and Ni (1 corresponds to Ga, 2 to Ta, and 3 to Ni); (b) element distribution of Au, O, and Ti (1 corresponds to Ti, 2 to Au, and 3 to O).

bedded onto the GaN epilayer. Fourier transform for GaN [Fig. 7(c)] was important to calibrate the HREM image. It was necessary also to determine the *d* spacing of the lattice fringes observed in the Fourier transform of the Au–Ni/(Ti,Ta)N microstructure [Fig. 7(b)]. An analysis of the calculated *d* spacing and angles between the diffraction spots of Fig. 7(b) demonstrates that both Au–Ni and (Ti,Ta)N compounds have cubic unit cells with $a_{\text{Au-Ni}} = 3.64 \text{ \AA}$ and $a_{\text{(Ti,Ta)N}} = 4.30 \text{ \AA}$, respectively. The following epitaxial relationships can thus be established: $(111)\text{Au-Ni} \parallel (0002)\text{GaN}$; $[0\bar{1}1]\text{Au-Ni} \parallel [2\bar{1}10]\text{GaN}$, and $(111)\text{(Ti,Ta)N} \parallel (0002)\text{GaN}$; $[0\bar{1}1]\text{(Ti,Ta)N} \parallel [2\bar{1}10]\text{GaN}$.

As discussed earlier, the unit cell parameters of alloys depend on the ratio of the components, and that these parameters increase with the increasing fraction of atoms having larger ionic radii. Based on this, it may be concluded that the approximate composition of the $\text{Au}_x\text{Ni}_{1-x}$ alloy was between $\text{Au}_{0.08}\text{Ni}_{0.92}$ ($a_{\text{Au}_8\text{Ni}_{92}} = 3.58 \text{ \AA}$) and $\text{Au}_{0.50}\text{Ni}_{0.50}$ ($a_{\text{Au}_{50}\text{Ni}_{50}} = 3.84 \text{ \AA}$), respectively. Based on similar parameters for the TiN and the $\text{Ti}_{0.25}\text{Ta}_{0.25}\text{N}_{0.50}$ alloys, which are $a_{\text{TiN}} = 4.24 \text{ \AA}$ and $a_{\text{Ti}_{25}\text{Ta}_{25}\text{N}_{50}} = 4.33 \text{ \AA}$, respectively, one can conclude that the mole fraction *x* for $\text{Ti}_x\text{Ta}_{0.5-x}\text{N}_{0.50}$ was $0 < x < 0.25$. The thickness of the Ti–O layer on the surface of the Ohmic contact was between 55 and 75 nm (see Fig. 5).

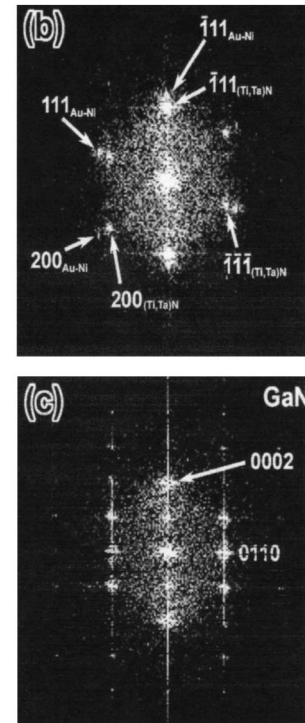
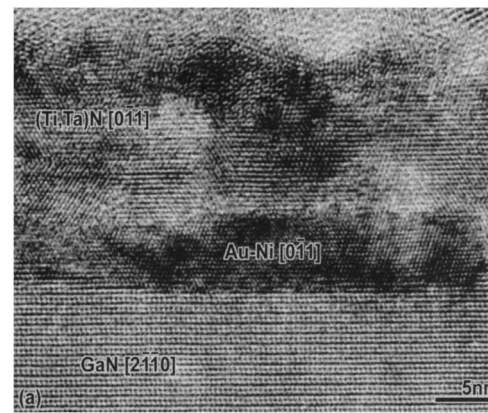


FIG. 7. (a) HREM image of an interface between GaN and the Ohmic contact formed after annealing at 750 °C (sample 3). Fourier transforms of (b) (Ti,Ta)N/Au–Ni and (c) GaN areas allow determination of epitaxial relationships and approximate Ti:Ta and Au:Ni ratios.

The BF image (Fig. 8) and the EDX spectra (Fig. 9) taken across the sample 5 Ohmic contact reveal the formation of four distinct layers upon RTA. The first one was a pseudocontinuous layer, about 35 nm thick, of the Au–Ta alloy crystal embedded onto GaN. The Au migration to the M/S interface is almost 90%. The second one was (Ti,Ta)N, about 5–8 nm thick, formed on the surface of the GaN epilayer. Analysis of HREM images from the GaN/Au–Ta/(Ti,Ta)N interface regions indicated that the Au–Ta and the (Ti,Ta)N alloys have cubic unit cells with $a_{\text{Au-Ta}} = 4.11 \text{ \AA}$ and $a_{\text{(Ti,Ta)N}} = 4.29 \text{ \AA}$, respectively. This corresponds to $\text{Au}_{0.90}\text{Ta}_{0.10}$ and $\text{Ti}_x\text{Ta}_{1-x}\text{N}_{0.50}$ with $0 < x < 0.25$. Both layers grow epitaxially on the GaN *c*-plane with epitaxial relationships: $(111)\text{Au}_{0.90}\text{Ta}_{0.10} \parallel (0002)\text{GaN}$; $[0\bar{1}1]\text{Au}_{0.90}\text{Ta}_{0.10} \parallel [2\bar{1}10]\text{GaN}$, and $(111)\text{Ti}_x\text{Ta}_{1-x}\text{N}_{0.50} \parallel (0002)\text{GaN}$; $[0\bar{1}1]\text{Ti}_x\text{Ta}_{1-x}\text{N}_{0.50} \parallel [2\bar{1}10]\text{GaN}$.

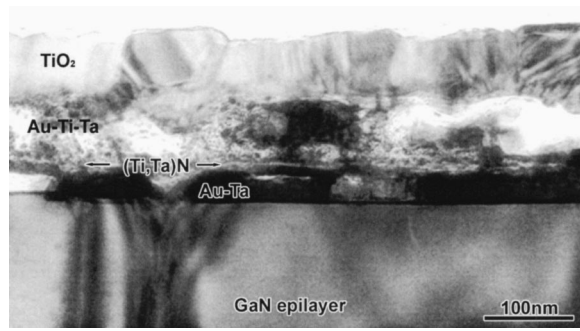


FIG. 8. TEM bright-field (BF) image of sample 5 annealed at 775 °C showing the Ta–Au alloy on the top of the GaN epilayer. (Ti,Ta)N lies on the top of Ta–Au.

Unlike the sample 3 Ohmic contact, where the Ni–Ga alloy was observed as a third layer formed on the top of the $Ti_xTa_{1-x}N_{0.50}$ alloy, the sample 5 Ohmic contact had two typical compositions within the third layer, alternating in lateral dimension. The first one, depicted in Fig. 8, was a polycrystalline ternary Au–Ti–Ta alloy layer with crystallite sizes typically in the range of several tens of a nanometer. As evident from Fig. 8, the thickness and the lateral dimension of grains with this composition were 60–70 nm and 2–5 μm , respectively. The second grain (not shown here) consisted of the Ni–Ga–Au–Ta alloy with 100–200 nm in lateral size. The layer thickness was 60–110 nm. The lateral size of the grains with this composition was usually around 1 μm .

Ti atoms outdiffused during RTA both at 750 and 775 °C forming titanium oxide, about 55–85 nm thick, on the top of the Ohmic contact. The EEL spectra of the top Ti–O layer of samples 3 and 5 revealed that Ti was octahedrally coordinated with oxygen atoms forming the TiO_2 alloy.^{23,24} However, this TiO_2 was present in relatively low concentration in sample 3, with most of the oxygen dissolved in titanium forming an oxygen reduced TiO_{2-x} phase or (Ti,O) solid solution. We believe that the formation of the dielectric TiO_2 layer at the contact surface is one of the possible reasons for an order of magnitude higher resistivity of the sample 5 Ohmic contact than that of the sample 3 Ohmic contact.

D. Overall Ta/Ti/Ni/Au microstructure analysis

The Ta/Ti/Ni/Au (50 Å/500 Å/200 Å/150 Å) microstructure demonstrated low contact resistivity in the range of $5 \times 10^{-6} \Omega \text{ cm}^2$ after RTA at 750 °C for 45 s. This contact resistivity of the contacts was comparable to that of the Ti/Al-based contacts.⁵ The design rationale underlying this contact was to utilize the combined nitride forming effect of Ti and Ta, in order to obtain an improved tunneling contact configuration. Because of the absence of Al in the microstructure, it was thought that the metallization would be thermally stable. However, although contact resistivity was low at room temperature, it degraded under high temperature thermal stressing, as evident from the following discussion.

XRD spectra of the contacts annealed at 750 °C showed the presence of Au(Ni,Ti) amorphous solid solutions. These spectra predicted also the presence of metal nitrides, (Ti, Ta)N, formed in the microstructure upon RTA at 750 °C for

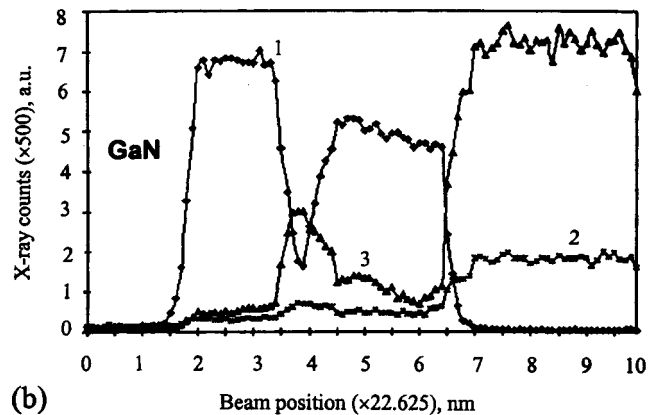
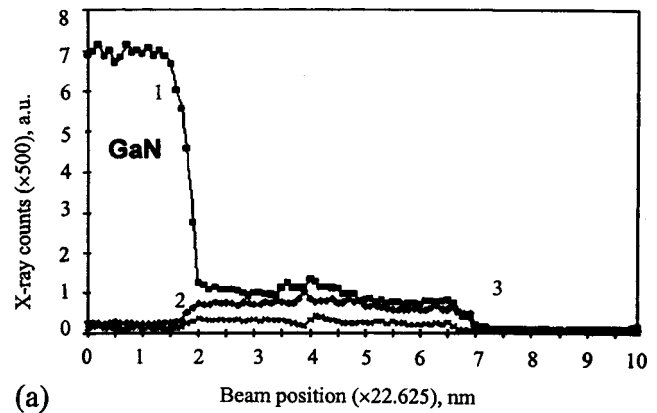


FIG. 9. EDX line profile spectra showing the element distribution across the Ohmic contact; (a) signal for Ta, Ga, and Ni (1 corresponds to Ga, 2 to Ta, and 3 to Ni); and (b) signal for Au, O, and Ti (1 corresponds to Au, 2 to O, and 3 to Ti). Note the near absence of the signal from Ni.

45 s. Although the XRD data did not conclusively confirm the presence of metal nitrides in the microstructure, these could not altogether be ruled out. In fact, based on TEM, the formation of (Ti,Ta)N alloys appeared quite plausible, which led to the creation of nitrogen vacancies in the crystal lattice. Heavy doping and carrier degeneracy, consequently, followed. The contact resistivity was thus lowered.

Cross-sectional TEM images of the Ta/Ti/Ni/Au (5 nm/50 nm/20 nm/15 nm) sample deposited on *n*-GaN and annealed at 750 and 775 °C, respectively, for 45 s suggested extensive in- and outdiffusion of metal atoms. Consumption of some of the GaN layer, which led to the formation of the $Ti_xTa_{1-x}N_{0.50}$ ($0 < x < 0.25$) alloy at the GaN interface, was observed in the Ta/Ti/Ni/Au (5 nm/50 nm/20 nm/15 nm) structure annealed both at 750 and 775 °C. Almost an order of magnitude lower contact resistivity measured for sample 3 annealed at 750 °C can, at least partly, be attributed to the structure and the chemical bonding differences of the two Ti–O layers formed on the contact surfaces as revealed by the EEL spectra.

The structures of samples 3 and 4 are identical. However, while sample 3 was annealed at 750 °C for 45 s, sample 4 was annealed at 750 °C for 60 s. RTA for a longer period, but at the same temperature, led to an increase in resistivity by almost an order of magnitude. Samples 4 and 5 have resistivities in the same order of magnitude. If the RTA time

and RTA temperature of sample 3 are considered to be optimum, then a comparison may be made of samples 3 and 4 and, of samples 3 and 5. This comparison demonstrates that an increase in RTA time and of RTA temperature had identical effects. RTA at 750 °C for 45 s created a combination of TiO₂ and TiO on the contact surface. In contrast, both RTA at 775 °C for 45 s and RTA at 750 °C for 60 s resulted in higher resistivity. An inspection of sample 3: Ta/Ti/Ni/Au (5 nm/50 nm/20 nm/15 nm) contact, sample 7: Ta/Ti/Ni/Au (8 nm/50 nm/20 nm/15 nm) contact, and sample 9: Ta/Ti/Ni/Au (2.5 nm/50 nm/20 nm/15 nm) contact, all annealed at 750 °C for 45 s indicates that, while a thicker Ta layer had a minor adverse effect, a thinner Ta layer had a major adverse effect, on the contact resistivity.

V. THERMAL STABILITY

The thermal stability of the Ta/Ti/Ni/Au (50 Å/500 Å/200 Å/150 Å) microstructure annealed at 750 °C was studied. Contacts were thermally stressed at 400 °C for 24 h. TLM and I - V measurements were made before and after the heat treatment. The I - V characteristic curves of the contacts before and after heat treatment are presented in Figs. 10(a) and 10(b), respectively. Figures 10(a) and 10(b) show that the contacts suffered from degradation after aging at 400 °C for 24 h. Degradation of the microstructure can best be explained on the basis of the AES depth profile of the contacts annealed at 750 °C (see Fig. 4), and the TEM images of the contacts annealed at 750 and 775 °C (see Figs. 5 and 8), respectively. It was revealed that upon annealing, Ti had out-diffused through the Ni layer, and that it was exposed to the surface, where it reacted rapidly with oxygen, yielding a thin coating of Ti_xO_y on the contact surface. Ti is known to form oxides even with a very low concentration of oxygen in the environment. As the reaction proceeded, more Ti diffused outwards to form Ti oxides. Thus, the oxidation reaction entirely consumed Ti that arrived at the surface. This reaction was thermodynamically favorable, and was the driving force behind the extensive outdiffusion of Ti towards the contact surface. Formation of Ti oxides at the surface appears to be the primary cause of the degradation of the contact microstructure, when subjected to thermal stress for 24 h.

The present study demonstrated that the effect of diffusivity of metals into one another is extremely important, and that it must be carefully taken into consideration while designing Ohmic contacts for high temperature applications. The role of diffusion barriers must at least be born in mind while designing these contacts.

As the Ti layer was overlaid first with 200-Å-thick Ni and next with 150-Å-thick Au, Ti was thought to be protected from oxidation during RTA. In fact, it was indeed protected until thermal stressing at elevated temperatures enhanced the oxidation reaction of Ti. It is the oxidation reaction kinetics of Ti, which led Ti to be dragged in large amounts to the surface upon thermal stressing. Therefore, the very cause of degradation was actually the enhanced diffusivity of Ti through Ni due to increased oxidation of Ti at the surface. The immediate consequence of this was the dramatic failure of the contacts at elevated temperatures. Hence, for

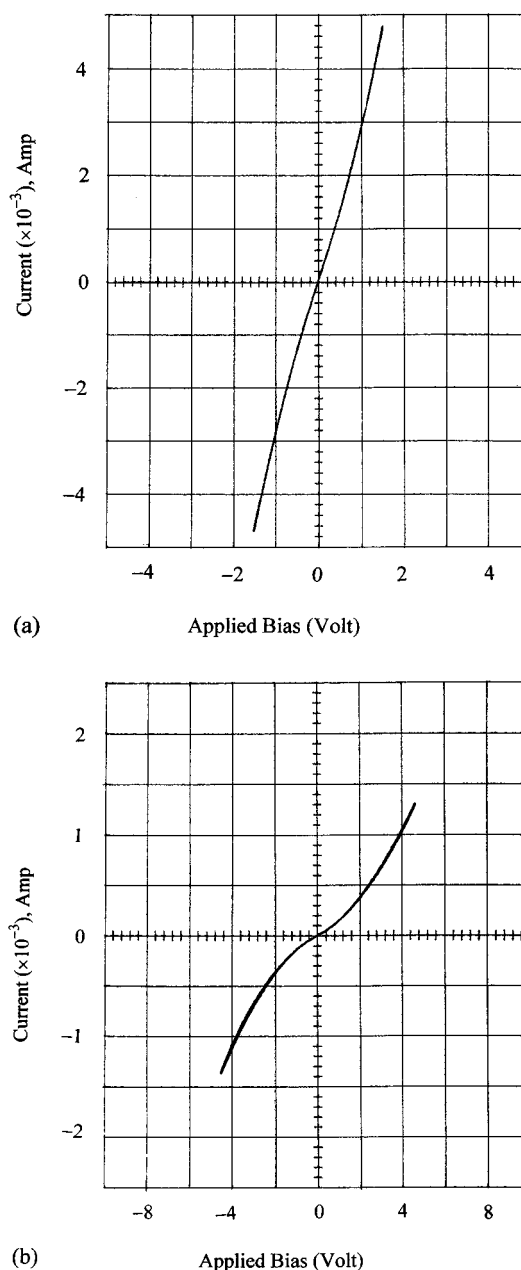


FIG. 10. Comparison of the I - V characteristic curves of the Ta/Ti/Ni/Au (50 Å/500 Å/200 Å/150 Å) microstructure contacts (annealed at 750 °C for 45 s) (a) before thermal stressing and (b) after thermal stressing at 400 °C for 24 h.

designing the alloyed Ohmic contacts, reaction kinetics must be taken into consideration very seriously. It must be realized that these are the ones that dictate the ultimate electrical, microstructural, chemical, and physical characteristics of the contacts. Similar causes affected the failure of Ti/Au/Pd/Au contacts.²¹ Observation of identical trends of the failure mechanism observed during thermal stressing of several different Ti microstructures is important in the sense that it provides directions to the designing of thermally stable Ohmic contacts. The purpose of the Ni overlayer was to act as a diffusion barrier against the outdiffusion of Ti and indiffusion of Au. Unfortunately, it performed poorly in both cases. It did not work well in preventing diffusion of Au toward the M/S interface. The diffusivity of Ti was too high

upon stressing at high temperatures, and Ni could not prevent it from outdiffusion towards the contact surface.

VI. CONCLUSION

Both the AES depth profile and TEM images for the annealed contacts suggested that Ni performed poorly as a diffusion barrier. It could not prevent inward diffusion of the top Au layer into the Ta/Ti bilayer, and also into the *n*-GaN epilayer underneath it, during RTA. As a result, thermal alloying at elevated temperatures led to the formation of several Au-based solid solutions embedded on the GaN epilayer and on other parts of the microstructure. It was revealed that, upon RTA, the *n*-GaN/Ta/Ti/Ni/Au system yielded the (Ta, Ti)N alloy in the vicinity of the metal/*n*-GaN interface. A tunneling contact configuration was thus formed near the metal/GaN interface. The contact resistivity of the optimum contact (for example, the sample 3 contact) was low, implying that, for this contact, probably tunneling dominated the transport mechanism at the M/S interface. The *n*-GaN film employed for the present metallization had a relatively low doping level (e.g., $5 \times 10^{17} \text{ cm}^{-3}$). Hence, the heavy doping in the sample 3 and 7 contacts was the result of N vacancies formed during the alloying of $\text{Ti}_x\text{Ta}_{1-x}\text{N}_{0.50}$ ($0 < x < 0.5$), about 5–9 nm thick. Only a few monolayers of this $\text{Ti}_x\text{Ta}_{1-x}\text{N}_{0.50}$ alloy were sufficient to create about 100 Å of heavily doped GaN with a density of $\sim 10^{20} \text{ cm}^{-3}$. TEM micrographs confirmed that N-rich $\text{Ti}_x\text{Ta}_{1-x}\text{N}_{0.50}$ alloys were indeed formed in the samples during RTA. So, it may be concluded that two factors significantly influenced the contact resistivities of the Ta contacts. These are the detrimental effect of the Ti–O layer formed on the contact surface, and the heavy doping of the GaN subsurface due to N vacancies. In order to accomplish acceptable performance, the oxidation reaction of Ti should be minimal and the concentration of nitrogen vacancies should be maximum.

It is known that, at high annealing temperature, Al tends to ball up,²⁵ resulting in a rough contact morphology. So, in order to develop thermally stable Ohmic contacts, low work-function alloys of refractory metals such as W, Ta, and Ni must be used. Ta, with a melting point as high as 3738 °C, is probably a reasonable choice for such metallization. Ta/Ti contacts to *n*-GaN annealed at high temperatures produced fairly low Ohmic contact resistivity. The very success of these contacts is rooted in the fact that, at high annealing temperatures, Ti and Ta reacted to form (Ta,Ti)N alloys. The success of the contact relied also on the Ta-to-Ti ratio of the contacts. If this ratio is such that Ta is too small as compared to Ti, and that Ta, rather than Ti, will be consumed fully in a reaction to form (Ta,Ti)N, then the remaining Ti would tend, at high temperatures, to outdiffuse, forming Ti oxide on the metal surface. If Ta and Ti layer thicknesses are so optimized that both Ta and Ti will be consumed fully in reacting with N to form the (Ta,Ti)N alloys, nitrogen vacancies in sufficient numbers will be formed. Earlier investigations^{26,27} of the effect of Al-to-Ti ratios: 1.1, 2.1, 3.5, and 5.4, demonstrated that a larger Al-to-Ti ratio had better thermal stability. This study clearly suggested that the presence of low work-function Al_3Ti , which was formed as a result of reaction

between Al and Ti, and which consumed essentially the entire Ti layer at high annealing temperatures, is favorable for good Ohmic contact. A similar study of the Ta-to-Ti ratio would shed light on the thermal stability of Ta/Ti/Ni/Au contacts.

ACKNOWLEDGMENTS

The research was carried out for partial fulfillment of Ph.D. dissertation for one of the authors (A.M.), and was supported by U.S. Army Research Laboratory Contract No. DAAD17-00-C-0092 and BMDO Contract No. N00014-01-1-1082. The authors wish to thank Dr. D. Webb (NRL) for discussions, and Tony Gomez, Crawford Taylor, and Urmi Motayed for technical assistance.

- ¹J. S. Foresi and T. D. Moustakas, *Appl. Phys. Lett.* **62**, 2859 (1993).
- ²M. Asif Khan, M. S. Shur, and Q. Chen, *Electron. Lett.* **31**, 2130 (1995).
- ³N. A. Papanicolaou, A. Edwards, M. V. Rao, J. Mittereder, and W. T. Anderson, *J. Appl. Phys.* **87**, 380 (2000).
- ⁴T. Gressmann, T. L. Li, E. L. Waldron, J. W. Graff, E. F. Schubert, and J. K. Sheu, *Appl. Phys. Lett.* **80**, 986 (2002).
- ⁵B. P. Luther, S. E. Mohny, T. N. Jackson, M. A. Khan, Q. Chen, and J. W. Yang, *Appl. Phys. Lett.* **70**, 57 (1997); see, also, Q. Z. Liu and S. S. Lau, *Solid-State Electron.* **42**, 677 (1998).
- ⁶S. Heikman, S. Keller, S. P. DenBaars, and U. K. Mishra, *Appl. Phys. Lett.* **78**, 2876 (2001).
- ⁷J. Burm, K. Chu, W. A. Davis, W. J. Schaff, T. J. Eutis, and L. F. Eastman, *Appl. Phys. Lett.* **70**, 464 (1997).
- ⁸Z.-F. Fan, S. Noor Mohammad, W. Kim, O. Aktas, A. E. Botchkarev, and H. Morkoç, *Appl. Phys. Lett.* **68**, 1672 (1996).
- ⁹D.-F. Wang, F. Shiwei, C. Lu, A. Motayed, M. Jah, S. Noor Mohammad, K. A. Jones, and L. Salamanca-Riba, *J. Appl. Phys.* **89**, 6214 (2001).
- ¹⁰A. Motayed, R. Bathe, M. C. Wood, O. S. Diouf, R. D. Vispute, and S. Noor Mohammad, *J. Appl. Phys.* **93**, 1087 (2003).
- ¹¹A. Motayed, A. V. Davydov, L. A. Bendersky, M. C. Wood, M. A. Derenge, D. F. Wang, K. A. Jones, and S. Noor Mohammad, *J. Appl. Phys.* **92**, 5218 (2002).
- ¹²C. Lu, H. Chen, X. Lv, X. Xie, and S. Noor Mohammad, *J. Appl. Phys.* **91**, 9218 (2002).
- ¹³D. Qiao, L. Jia, L. S. Yu, P. M. Asbeck, S. S. Lau, S.-H. Lim, Z. Liliental-Weber, T. E. Haynes, and J. B. Barner, *J. Appl. Phys.* **89**, 5543 (2001).
- ¹⁴S.-H. Lim, J. Washburn, Z. Liliental-Weber, and D. Qiao, *Appl. Phys. Lett.* **78**, 3797 (2001).
- ¹⁵S. Ruvimov, Z. Liliental-Weber, J. Washburn, K. J. Duxstad, E. E. Haller, Z.-F. Fan, S. Noor Mohammad, W. Kim, O. Aktas, A. E. Botchkarev, and H. Morkoç, *Appl. Phys. Lett.* **69**, 2582 (1996).
- ¹⁶M. Suzuki, T. Kawakami, T. Arai, S. Kobayashi, Y. Koide, T. Uemura, N. Shibata, and M. Murakami, *Appl. Phys. Lett.* **74**, 275 (1998).
- ¹⁷H. Ishikawa, S. Kobayashi, and Y. Koide, *J. Appl. Phys.* **81**, 1315 (1997).
- ¹⁸*Handbook of Thermionic Properties*, edited by V. S. Fomrenko and G. V. Samsonor (Plenum, New York, 1966); see, also, T. C. Shen, G. B. Gao, and H. Morkoç, *J. Vac. Sci. Technol. B* **10**, 2113 (1992).
- ¹⁹Y. Kasukabe, *J. Vac. Sci. Technol. A* **15**, 1848 (1997).
- ²⁰L. B. Pankratz, J. M. Stuve, and N. A. Gokcen, *Thermodynamic Data for Mineral Technology* (Bureau of Mines, Washington, DC, 1984), p. 355.
- ²¹A. Motayed and S. Noor Mohammad (unpublished).
- ²²Z. Liliental-Weber, Y. Chen, S. Ruvimov, and J. Washburn, *Phys. Rev. Lett.* **79**, 2835 (1997).
- ²³D. N. Zakharov, Z. Liliental-Weber, A. Motayed, and S. Noor Mohammad, *Mater. Res. Soc. Symp. Proc.* **764**, C3.17.1 (2003).
- ²⁴R. Brydson, L. A. J. Garvie, A. J. Cravent, H. Sauer, F. Hofer, and G. Cressey, *J. Phys.: Condens. Matter* **5**, 9379 (1993).
- ²⁵Y. Wu, W. Jiang, B. Keller, S. Keller, D. Kapolnek, S. DenBaars, and U. K. Mishra, *Proceedings of the Workshop on III–V Nitrides*, Nagoya, Japan (1995).
- ²⁶M. H. Tsai, S. C. Sun, H. T. Chiu, C. E. Tsai, and S. H. Chuang, *Appl. Phys. Lett.* **67**, 1128 (1995).
- ²⁷B. P. Luther, S. E. Mohny, and R. F. Karlcek, *Proceedings of the 39th Electronic Materials Conference*, Fort Collins, CO, 25–27 June (1997).